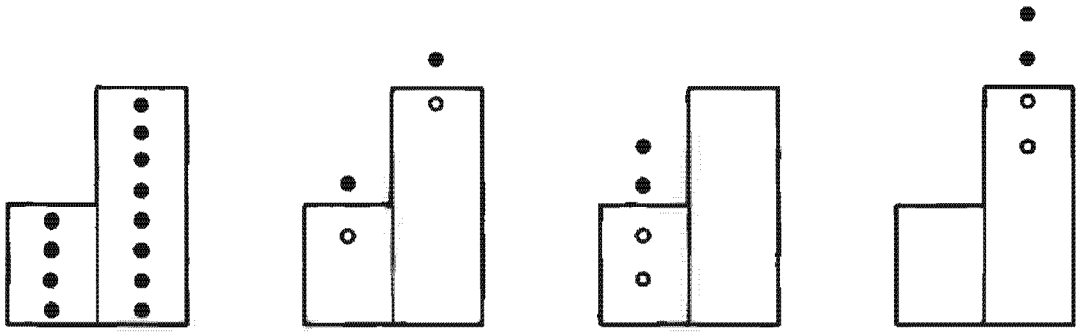

Figure 2.10. Schematic representation of shell model configurations.

From Fig. 2.10a we see that a shell model state where all occupied proton levels are also occupied by neutrons has $T = T_3$, because operating with $T_+ = \sum_i t_+^{(i)}$ onto this state gives 0, that is, this state has the maximal value of T_3 for a fixed value of T. This shows in particular that the shell model ground state for $N = Z$ nuclei has $T = 0$.

For non-magic heavy nuclei the shell model ground state is certainly not a good approximation to the exact ground state. There are admixtures of $1p$-$1h$, $2p$-$2h$ states. As we will show in Chapter 5, the construction of a self-consistent, one-particle potential assures that there are no $1p$-$1h$ admixtures. Since the shell model potential is a good approximation to such a potential, we neglect these contributions here and argue about $2p$-$2h$ admixtures. Furthermore, we assume that $\Delta_c \simeq \hbar\omega_0$, which is the case for heavy nuclei like ^{208}Pb, and neglect $2p$-$2h$ configurations with an unperturbed energy larger than $2\hbar\omega_0$. As we see from Fig. 2.10b, c, d there are three types of configurations. Only type b contains configurations which violate the isospin, namely, those where the proton particle sits in the same level as the neutron hole. The ratio of the number of these configurations to the number of all configurations of type b is $1/(N-Z)$, where $(N-Z)$ is the neutron excess. If we make the statistical assumption that all these configurations are admixed with the same weight, we find that the isospin impurity in the ground state of heavy nuclei is roughly $1/(N-Z)$. Similar considerations apply for excited states, and we find that heavy nuclei with large neutron excesses have rather pure isospin. This result has also been found in more detailed investigations [LS 62, SK 65, KW 69, So 69, LM 74].

2.7 Comparison with Experiment

2.7.1 Experimental Evidence for Single-Particle (Hole) States

Besides the success of the shell model as an explanation of the magic numbers and angular momenta of the ground state, one would like to have direct experimental evidence for the nuclear shells. It turns out that direct stripping [e.g., (d, p)] and pickup (p, d) reactions, as well as direct $(p, 2p)$ and $(e, e'p)$ reactions, are well suited for this purpose. For example, a direct $(p, 2p)$ process is ideally one where the energy of the incoming proton is so high that it interacts only once with another proton in the

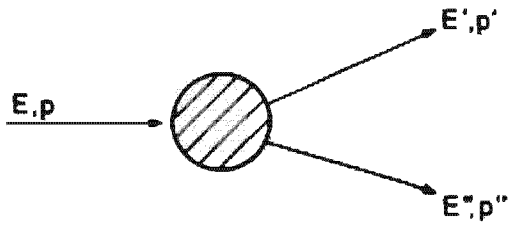

Figure 2.11. Schematic representation of the $(p, 2p)$ reaction.

nucleus, both protons leaving the nucleus without further interactions (Fig. 2.11).

Suppose that the knocked-out nucleon has been in a shell model state (Fig. 2.12). For its binding energy we have

$$E_B = E - E' - E''.$$

The cross section according to the shell model should have, as a function of the energy, resonances only at discrete values of E_B.

In reality, these resonances are broadened because of the influence of the residual interaction, as shown in Fig. 2.13 for the experimental cross section of ^{16}O $(p, 2p)$ ^{15}N. Nevertheless, one can clearly identify the

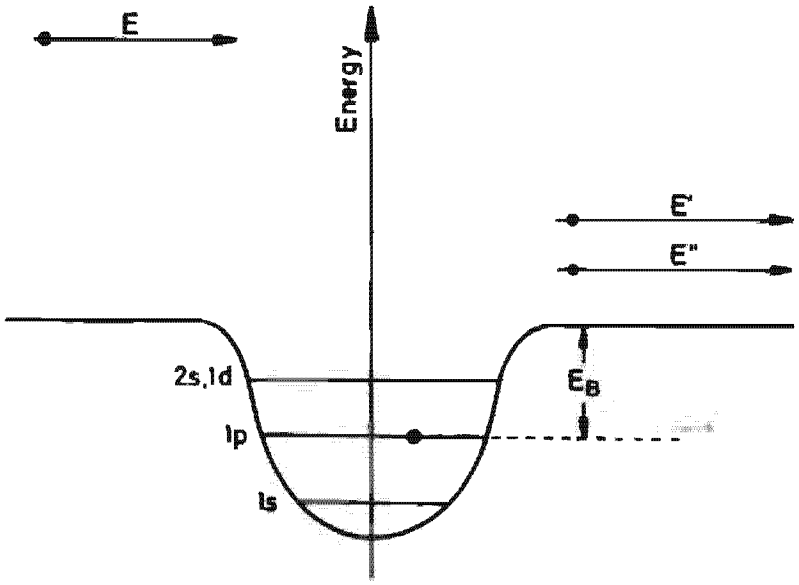

Figure 2.12. $(p, 2p)$ reaction in the shell model.

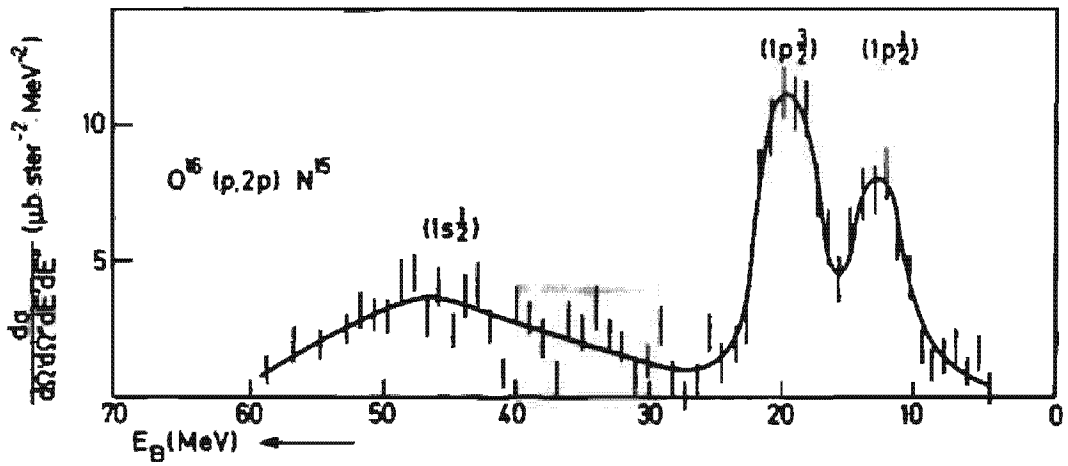

Figure 2.13. Experimental ^{16}O $(p, 2p)$ ^{15}N cross section [MHT 58].

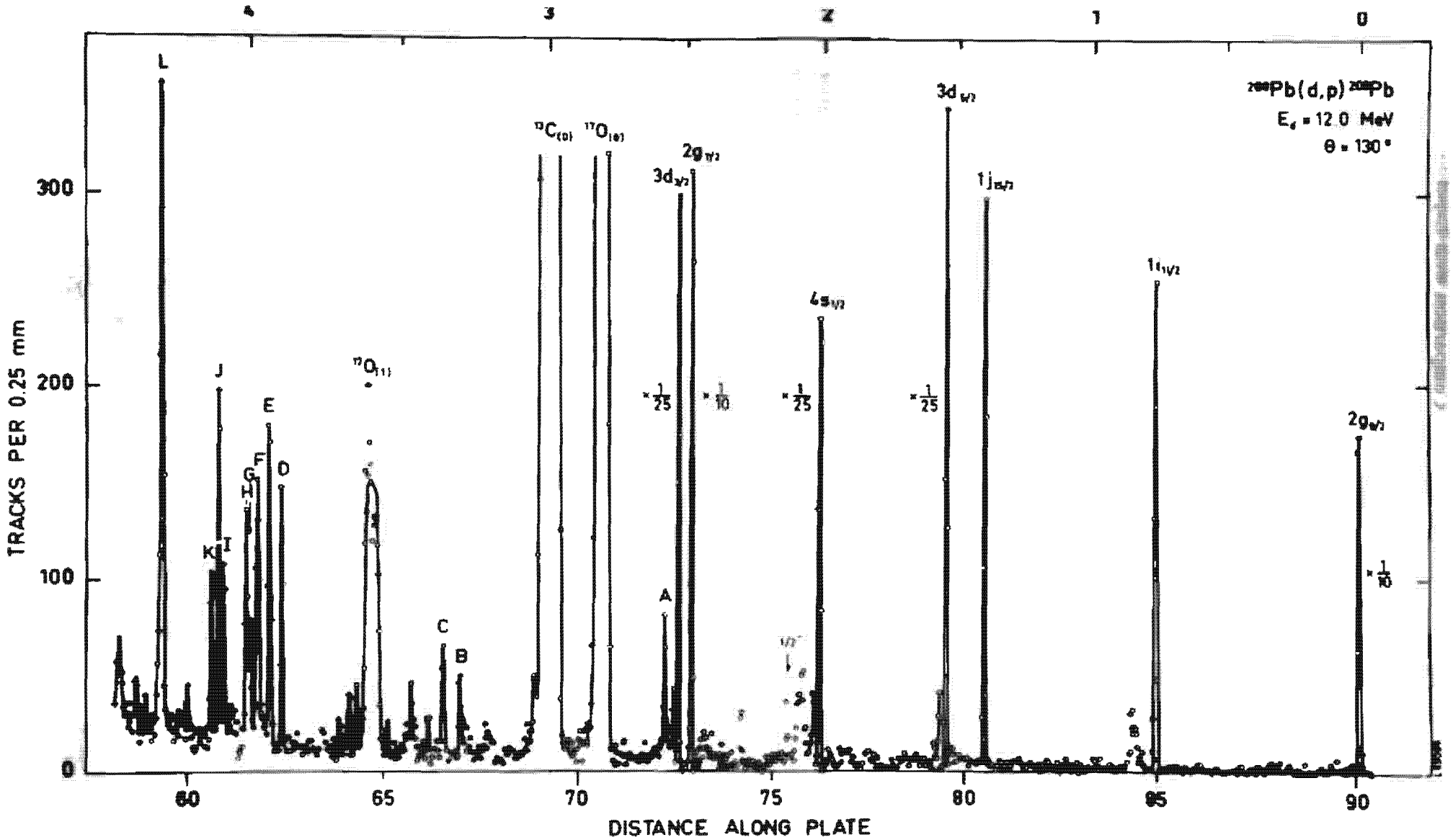

Figure 2.14. Neutron spectrum from the ^{208}Pb (d, p) ^{209}Pb reaction. The intensity peaks are labelled by their shell model assignment. (From[EKV 69]

$(\pi 1s_{1/2})$ level and the spin orbit split levels $(\pi 1p_{3/2})$ and $(\pi 1p_{1/2})$. Theoretical calculations for these reactions have been done by R. Lipperheide et al. [FLW 75].

In a similar manner, one can use stripping or pickup reactions like (d, p) and (p, d) to create neutron particle or neutron hole states, but the kinematical analysis has to be corrected for the binding of the deuteron. A nice example for neutron particle states in ^{209}Pb obtained with a (d, p) stripping reaction is presented in Fig. 2.14. It should be compared with Fig. 2.15, where experimentally determined proton and neutron single-particle energies for ^{208}Pb are shown in comparison with calculated levels, using a Woods–Saxon potential [BW 60].

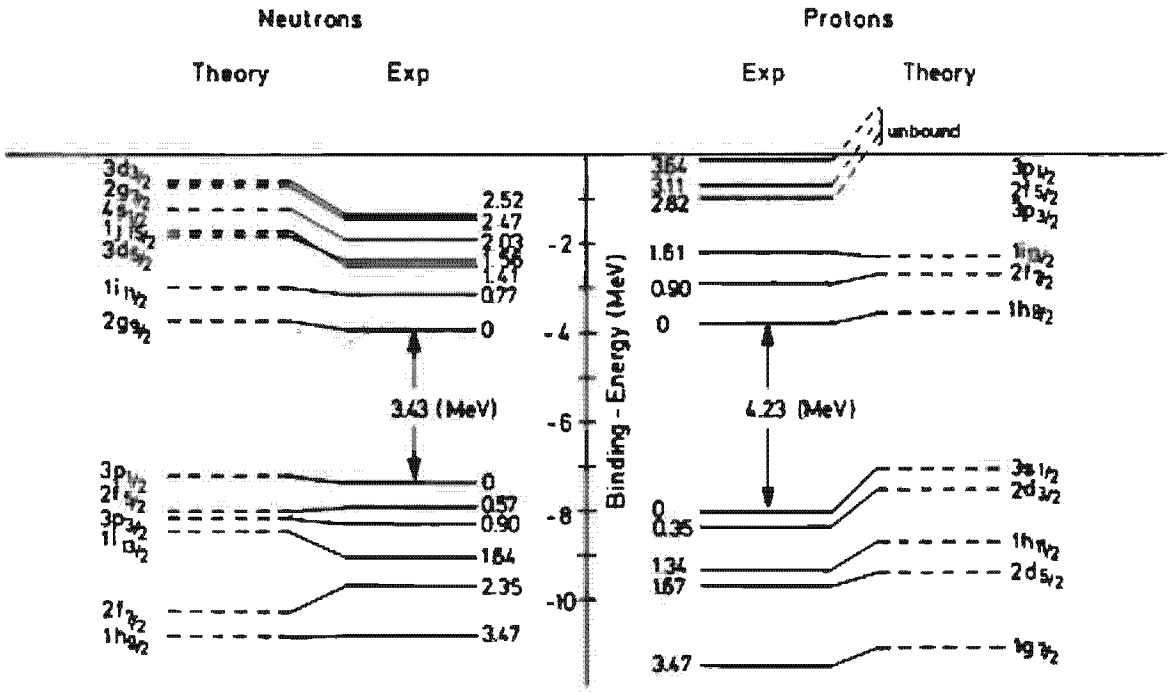

Figure 2.15. Comparison of experimental and calculated single-particle levels in ^{208}Pb.

One can show (see, for instance, [GL 70, Au 70, Ho 71b, EW 72]) that the absolute values of the cross sections of these reactions are proportional to the so-called spectroscopic factor

$$S_k = |\langle \Psi_{A+1} | a_k^+ | \Psi_A \rangle|^2, \tag{2.57}$$

where $|\Psi_A\rangle$, $|\Psi_{A+1}\rangle$ are the exact wave functions of the initial and final nucleus, and k stands for the quantum numbers of the observed single-particle state. If for the wave functions we use the pure shell model approximation, the spectroscopic factor is clearly equal to one.* However, if the wave functions contain admixtures of more complicated particle and hole configurations, which are introduced by the diagonalization of the residual interaction (2.35), the spectroscopic factor differs from one. Therefore, it is a measure of the purity of the single-particle states. The spectroscopic factors of the levels shown in Fig. 2.14 are in the range 0.8–0.9 (see, for instance, [RW 73]).

*This statement applies only for pure product states without angular momentum coupling. With angular momentum coupling, the different levels with different m values are partially filled and one has to take into account the Pauli principle.

2.7.2 Electromagnetic Moments and Transitions

Other important quantities ready for comparison with experiments are the electromagnetic moments and transition probabilities in odd mass nuclei. In a first approximation, one assumes that they are described by one external particle sitting on an inert core with even mass:

$$|\Phi_m\rangle = a_m^+ |\Phi_0\rangle, \tag{2.58}$$

where a_m^+ creates a particle in the level m and $|\Phi_0\rangle$ represents the wave function of the core (2.25).

The electromagnetic multipole operators $\hat{Q}_{\lambda\mu}$ and $\hat{M}_{\lambda\mu}$ (as defined in Appendix B), are one-particle operators. As shown in Appendix C, they can be represented as

$$\hat{Q} = \sum_{k_1 k_2} Q_{k_1 k_2} a_{k_1}^+ a_{k_2} \tag{2.59}$$

in the shell model basis. Using the Fermi commutation relations (C.23) for the operators a_k, a_k^+ and the fact that the levels m, m' are empty in the core ($a_m|\Phi_0\rangle = a_{m'}|\Phi_0\rangle = 0$), we get

$$\langle\Phi_m|\hat{Q}|\Phi_{m'}\rangle = \langle\Phi_0|\hat{Q}|\Phi_0\rangle\delta_{mm'} + Q_{mm'}. \tag{2.60}$$

The picture becomes especially simple if we assume that the core is a closed shell nucleus. In this case, all the electromagnetic matrix elements of the core ($I = 0$) vanish. The single-particle states are characterized by the quantum numbers $|k\rangle = |nljm\rangle$ and the electromagentic properties can be calculated from the matrix elements

$$Q_{kk'} = \langle nljm|\hat{Q}|n'l'j'm'\rangle, \tag{2.61}$$

which are given in Eqs. (B.81) and (B.82) of Appendix B.

For instance, we get the electromagnetic moments [(B.31) and (B.32)] as expectation values in the states $|nljm = j\rangle$ and the electromagnetic transition probabilities (B.72) from the reduced matrix elements of these operators.

Special care has to be taken in the case of single hole states (one particle less than a closed shell). As we have seen, they can be described in the same simple way as the single-particle states. Their wave function can be expressed by analogy with Eq. (2.58):

$$|\Phi_i\rangle = a_i|\Phi_0\rangle, \tag{2.62}$$

where $|\Phi_0\rangle$ is again the wave function of the core and a_i annihilates a particle in a level i occupied in $|\Phi_0\rangle$. By analogy with (2.60), we get

$$\langle\Phi_i|\hat{Q}|\Phi_{i'}\rangle = \langle\Phi_0|\hat{Q}|\Phi_0\rangle\delta_{ii'} - Q_{i'i}. \tag{2.63}$$

Since the electromagnetic multipole operators are self-adjoint in the sense of [Ed 57, Eq. (5.5.2)], the difference between (2.63) and (2.60) does not enter into the electromagnetic transition probabilities. However, in the case of electromagnetic moments, one has to take care of the sign in (2.63) and an additional phase. Since one is interested in the expectation value of a

state with angular momentum quantum numbers $j, m=j$, one has to create a hole in the level $|jm=-j\rangle$, which is proportional to the time-reversed level $T|jm=j\rangle$ [Eq. (2.45)]. Together with the minus sign in Eq. (2.63), one finds that hole states have the same magnetic moments as the corresponding particle states (the magnetic multipole operators are time odd), whereas the electric multipole moments of particle and hole states have different signs (the electric multipole operators are time even).

One example is the magnetic dipole moment (B.31)

$$\mu=\langle nljj|\mu_z|nljj\rangle=\sqrt{\tfrac{4\pi}{3}}\,\langle nljj|\hat{M}_{10}|nljj\rangle, \tag{2.64}$$

where the magnetic vector $\boldsymbol{\mu}$ is given by

$$\boldsymbol{\mu}=\mu_N\{g^l\mathbf{l}+g^s\mathbf{s}\}, \tag{2.65}$$

where $\mu_N=e\hbar/2mc$ is the nuclear magneton and g^l and g^s are the gyromagnetic rations for orbital angular momentum and spin ($g^l=1$, $g^s=5.586$ for protons and $g^l=0$, $g^s=-3.826$ for neutrons).

The magnetic moment μ can easily be calculated with the projection theorem for vector operators $\mathbf{A}$,

$$\langle jm|\mathbf{A}|jm'\rangle=\langle jm|\mathbf{j}|jm'\rangle\frac{\langle jj|\mathbf{A}\mathbf{j}|jj\rangle}{j(j+1)}, \tag{2.66}$$

which can be derived from the Wigner–Eckart theorem [Ed 57, Eq. (5.4.1)]. Applying it to the vector $\boldsymbol{\mu}$, we get

$$\begin{aligned}\mu&=\mu_N\frac{1}{j+1}\langle jj|g^l\mathbf{l}\mathbf{j}+g^s\mathbf{s}\mathbf{j}|jj\rangle\\&=\mu_N\frac{1}{2(j+1)}\left[g^l\left(j(j+1)+l(l+1)-\tfrac{3}{4}\right)+g^s\left(j(j+1)+\tfrac{3}{4}-l(l+1)\right)\right].\end{aligned} \tag{2.67}$$

For $j=l\pm\frac{1}{2}$ we get

$$\mu=\mu_N\begin{Bmatrix} g^l\left(j-\frac{1}{2}\right)+\frac{1}{2}g^s \\ \left[g^l\left(j+\frac{3}{2}\right)-\frac{1}{2}g^s\right]\frac{j}{j+1}\end{Bmatrix}\quad\text{for}\quad\begin{cases}j=l+\frac{1}{2}\\ j=l-\frac{1}{2}\end{cases}. \tag{2.68}$$

The functions $\mu(j)/\mu_N$ for $j=l\pm 1/2$ are called Schmidt lines (Figs. 2.16 and 2.17) (j can only take on discrete values $\mu(j)/\mu_N$, though it is shown here as a continuous function of j). The experimental values are given for comparison.

If the theory were exact, all μ-values would lie on the Schmidt lines and all orbital angular momenta $l=j\pm\frac{1}{2}$ would be determined. The experimental values, almost without exception, lie in between the two lines, most of them being grouped closer to one of the two lines. The l-values determined in this way almost always agree with those predicted by the shell model. The shell model should work best near magic numbers. Indeed, one finds close agreement, for example, for ^{15}N, ^{17}O, ^{39}K, ^{41}K, and ^{207}Pb. The

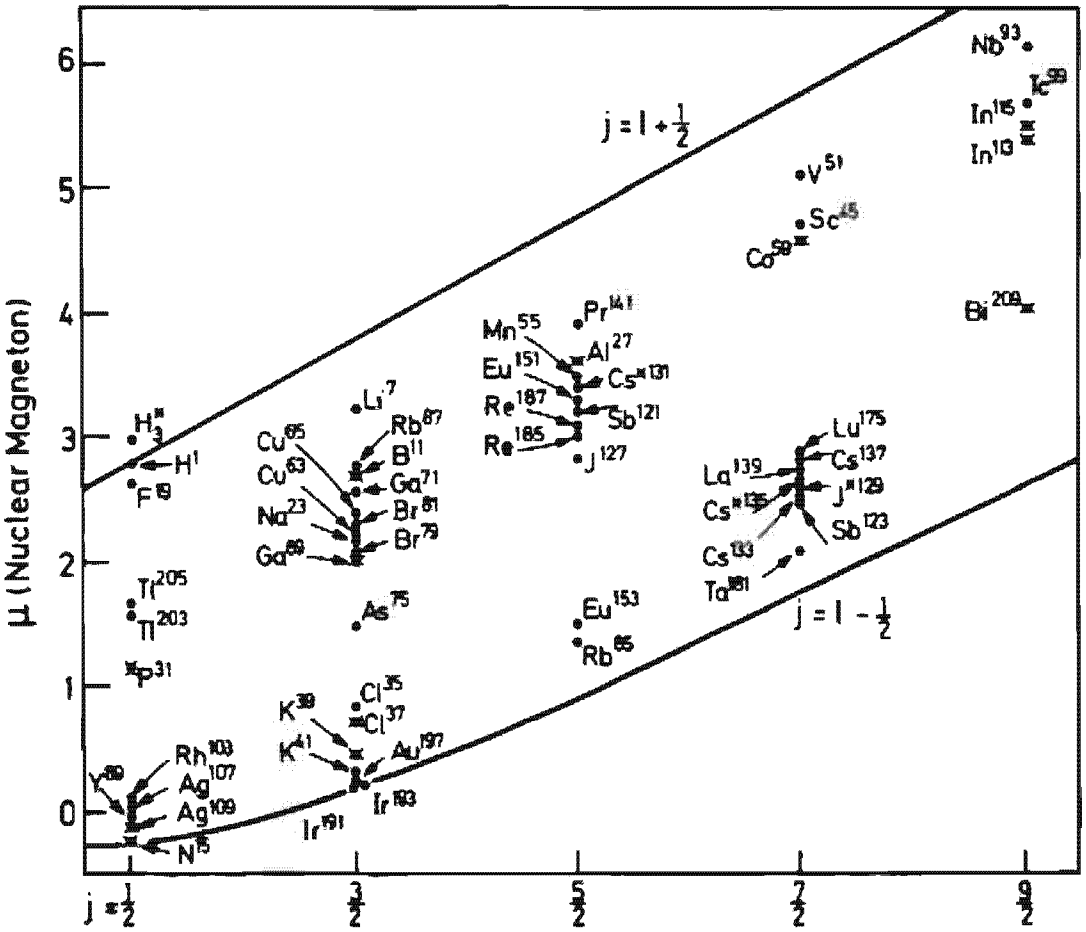

Figure 2.16. Magnetic moments for Z-odd nuclei as a function of angular momentum. (From [MJ 55].)

agreement is also not too bad for many nuclei far from closed shells. One can qualitatively understand this, because the magnetic moment in time-reversed levels is always of opposite sign. Since, as we shall see in Chapter 6, time-reversed levels are always occupied pair-wise, the most important contribution comes from the last odd particle. This is, however, only a

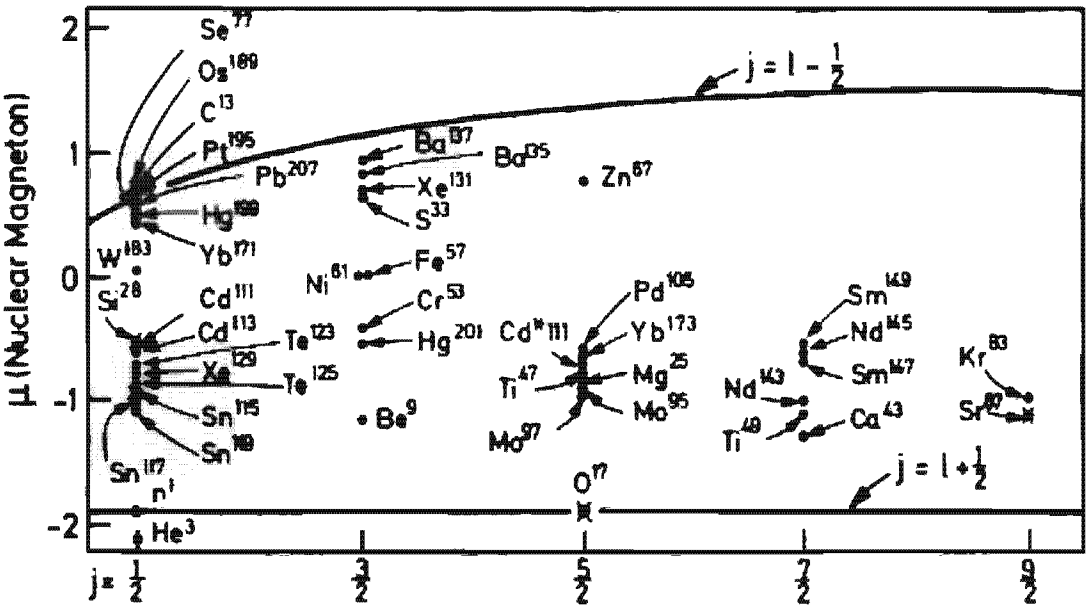

Figure 2.17. Magnetic moments of N-odd nuclei as a function of angular momentum. (From [MJ 55].)

qualitative argument and one also finds many deviations, especially for heavier nuclei, even in cases of rather pure one-particle or one-hole configurations.

There are two main reasons for these deviations:

(i) As we see in Appendix B, we have used the g-factors of bare nucleons in the calculation of the magnetic multipole operators. Within the nucleus however, there exist pionic currents between the nucleons that change these values, and effective g-factors, $\tilde{g}$, should be used.

(ii) The core usually does not stay inert in an external electromagnetic field. This can excite virtual vibrations which interact with the external particle. This effect is called a polarization of the core. To a large extent, it can be taken into account again by effective g-values. We will see in Section 9.3 how this polarization effect can be calculated microscopically.

The most important magnetic transitions are M1-transitions. In the pure single-particle model, the M1-operator (2.65) commutes with $\mathbf{l}^2$. This means that M1-transitions between levels with different l-quantum numbers are forbidden (l-forbidden transitions). In fact, such transitions are observed experimentally, but with a very small BM1-value. They cannot be understood by using only effective g-values, because one does not change the selection rules in this case. This clearly shows that mesonic effects (i) and polarizations (ii) produce not only vector components $\sim\mathbf{l}$ and $\sim\mathbf{s}$, but also more complicated effects. The simplest one is a "tensor component"

$$\delta\mu = \kappa r^2 [\, Y_2 \mathbf{s}\,]_1 t_3 . \tag{2.69}$$

By adjusting the constant κ in a reasonable way, one is able to describe these l-forbidden transitions quantitatively (see [BM 69, WB 69, and BSK 73]).

Let us come now to the electric properties. There are two important differences to the magnetic case:

(i) The electric operators are time-even. There are no cancellations of the contributions of time-reversed levels, but on the contrary they add up. This means that one cannot expect that the spherical single-particle model works outside the region of closed shells.

(ii) Since one can, in the long wavelength limit, (see Appendix B) neglect the contributions of currents to the electric multipole operators, we can use the conservation law for the electric charge and show that exchange effects do not play any role in the electric multipole operators. This means that apart from polarization effects, we can use the bare electric charge (*Siegert theorem* [Si 37]).

By analogy with the magnetic moment, one obtains for the electric quadrupole moment (B.81) of a single-particle state [EL 57, p. 255]

$$Q = e\sqrt{\frac{16\pi}{5}}\ \langle nljj|r^2 Y_{20}|nljj\rangle = -e\langle r^2\rangle \frac{2j-1}{2j+2}, \tag{2.70}$$

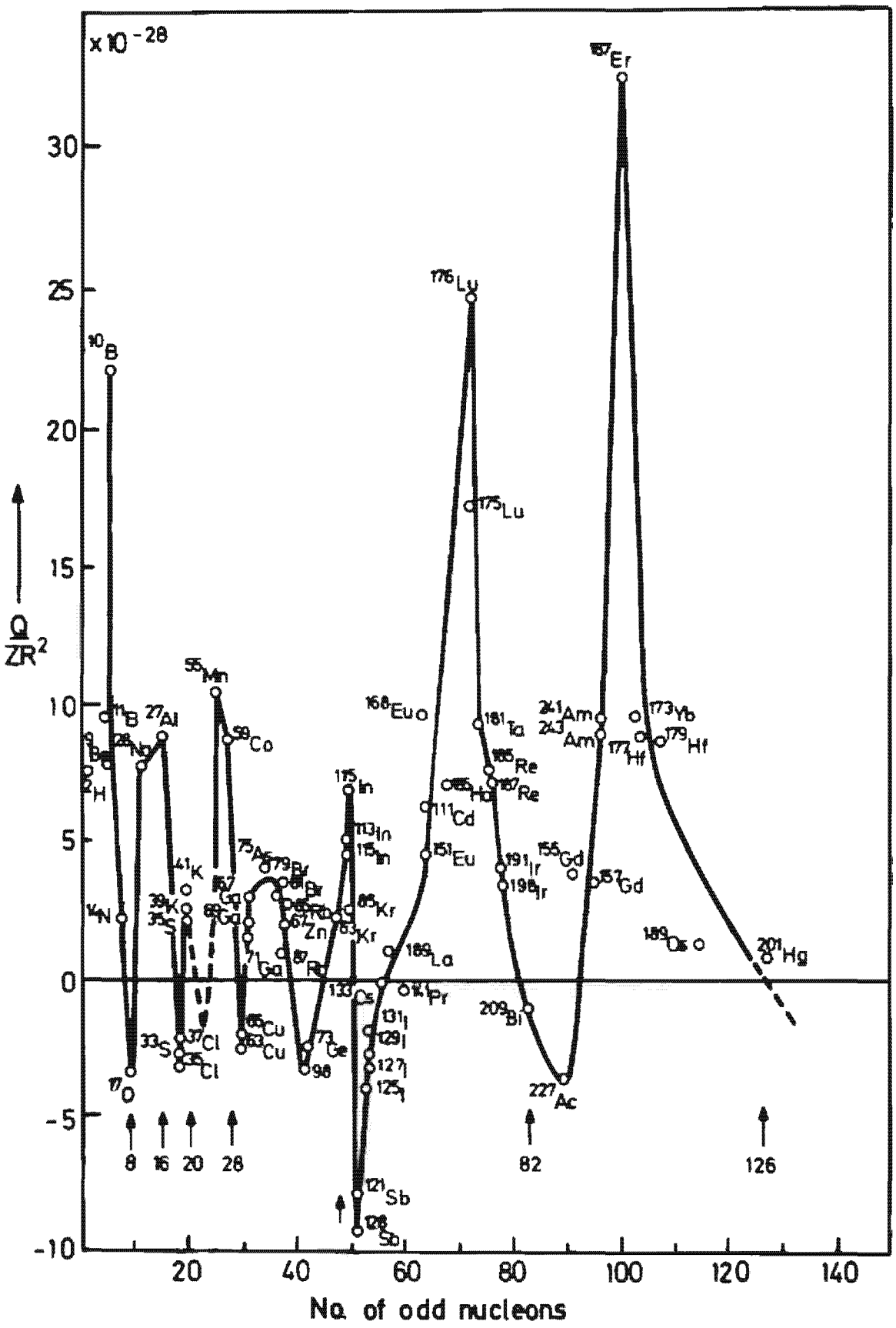

Figure 2.18. Quadrupole moments for odd-A nuclei against the number of odd nucleons. Arrows indicate closed shells. (From [Se 64].)

where $\langle r^2 \rangle$ is the average square radius of a particle in the state $|nljm\rangle$. For $j > 1/2$, the quadrupole moments turn out to be negative, that is, the probability distribution looks like a pancake in the plane perpendicular to the z-axis. For holes we have the opposite (i.e., prolate probability distributions). In Fig. 2.18, we see that this picture is qualitatively right in the neighborhood of magic numbers. However, as one fills the next shell with more and more nucleons, we soon find experimentally a transition to positive quadrupole moments with very large values. We shall see in the next chapter that in this case the average field of the nucleons is no longer spherical and we obtain a deformed density distribution. Only at the end of the shell, when nearly all levels are occupied, does one again get the picture of one or a few holes in a spherical core.

Even for one-particle or one-hole states with a magic core, this picture only gives qualitative agreement. Quantitatively, the measured quadrupole moments for proton states are roughly a factor of two larger than one would expect from (2.70) and values for neutron states do not vanish as they should according to Eq. (2.70), but behave as if the neutron had a charge. One usually expresses this fact by an effective charge e^{eff}. These effective charges can be explained by the polarization effect (see Sec. 9.3). Experimentally, it is observed that $e^{\text{eff}} \simeq 1$ for neutrons and $e^{\text{eff}} \simeq 2$ for protons.

The electric transitions behave very much like the corresponding moments. Only for the single-particle and single-hole nuclei near closed shells do they have values predicted by the single-particle shell model, with roughly the same effective charge as determined from the quadrupole moments.

Levels with *high angular momenta near closed shell* nuclei are often a mixture of only very few configurations (often there is only one configuration possible in a wide energy range). Sometimes—because of the selection rules of spin and parity—they can decay only by radiation with a high multipolarity. From Appendix B we learn that such transitions are highly suppressed because of kinematical factors. We therefore expect a very long lifetime for such nuclei. In fact, quite a few such "isomeric" states have been found in spherical nuclei (islands of isomers; see also Sec. 3.4.7).

2.8 Deformed Shell Model

2.8.1 Experimental Evidence

The assumption of approximately independent motion of nucleons in an average field is the basis of the shell model and of all microscopic theories of finite nuclei. This container potential is produced by the nucleons themselves and their mutual interaction. In Chapter 5 we shall see how to calculate this average potential. In its most simple form the potential well is spherical. This is true for nuclei with closed or nearly closed shells and, as we have seen in the last section, for such nuclei the spherical shell model